Opening up complete photonic bandgaps in three-dimensional photonic crystals consisting of biaxial dielectric spheres

Shiyang Liu*
Surface Physics Laboratory, Fudan University, Shanghai 200433, P. R. China

Zhifang Lin†
Department of Physics, Fudan University, Shanghai 200433, P. R. China

(Received 17 December 2005; revised manuscript received 7 April 2006; published 8 June 2006)

In this paper, the scattering matrix of sphere with dielectric biaxial anisotropy is obtained exactly within the framework of the extended Mie theory. By incorporating the scattering matrix into the multiple scattering method, we study theoretically the photonic band structure of three dimensional photonic crystals consisting of biaxial dielectric spheres. Our results demonstrate that complete photonic bandgaps can be found in both fcc and sc lattice structures, which are absent in photonic crystals composed of isotropic dielectric spheres. Moreover we have compared our results with those coming from the photonic crystals consisting of the uniaxially birefringent dielectric spheres. It is found that because of the enhancement of the anisotropy, the degeneracy is lifted further, resulting in two neighboring photonic bandgaps, the lower one is complete while the upper one is partial existing only in some special regions of the first Brillouin zone.

DOI: 10.1103/PhysRevE.73.066609 PACS number(s): 42.70.Qs, 42.25.Fx

I. INTRODUCTION

Photonic crystals (PCs) are composite structures with periodically modulated refractive index [1–4]. With the presence of the multiple scattering by the periodic structure and/or the appearance of the resonant mode of the building components, light propagating in PCs can be strongly modulated, which leads to the complicated band structure. If there exist complete photonic bandgaps (PBGs), light propagating can be absolutely forbidden and the spontaneous emission is prohibited within the frequency range of the PBGs. This property provides the ability to control the spontaneous emission and light propagation, which is of importance for both science and technology. The advance has resulted in many potential applications in optical and electronic devices such as selective reflectors, optical polarizers, band filters, semiconductor lasers, and solar cells [1,2,4–6].

It is therefore highly important to obtain a structure with complete PBGs. Considerable efforts have been made both in experimental and theoretical research works. It is well known that the contrast of dielectric constant, the shape of the dielectric structure and the topological connectivity of the dielectric materials play a crucial role in finding complete PBGs [5]. Previous studies concentrating on the isotropic constituents have proved that, for the PCs composed of spherical dielectric material, the complete PBGs can only be found in diamond structure and inverse opal face centered cubic structure [7–9]. The introduction of anisotropy, either in shape or in dielectricity can offer another chance to find PBGs in PCs [10,11]. Studies have been performed before within the framework of the plane wave expansion and the finite difference time domain method, the results have shown that in the two dimensions case anisotropy are effective in opening up the complete PBGs [13–15], yet in the three-dimensional case, the efficacy is limited [16,17]. A recent work has pointed out that through tuning, the orientation of the extraordinary axis of the birefringent dielectric spheres a complete PBG can be found in face centered cubic (fcc) and simple cubic (sc) lattices [11]. The above work suggests that, for the birefringent and biaxial dielectric materials, tuning the orientation of extraordinary axis renders us another freedom in modulating the photonic band structure and opening up complete PBGs.

In calculating band structures, the most frequently adopted technique is the pane-wave expansion method, which can offer reliable results in most cases. However, when a sharp change of electromagnetic wave occurs, it is difficult to achieve the convergence of the solution and sometimes the plane wave expansion method can even produce unreliable results, as pointed by Moroz [9] and Sözüer *et al.* [18]. Other techniques such as the transfer-matrix method and finite difference time domain method can also be used to calculate photonic band structures and possess the capability of conducting a general type of dielectric modulation [19–21]. Nevertheless, to achieve high accuracy at the boundary a fine mesh size will be necessary, thus requiring much more computer resources. Herein, we adopt multiple scattering method. Compared with other methods, multiple scattering method bears the advantages of numerical accuracy and computer time saving in calculating spherical scattering problems, since it takes into account the proper boundary conditions of the interface exactly. The multiple scattering method is also named as Koringa-Kohn-Rostoker method, which was originally developed for calculating the band structures of electrons [22,23] and was later extended to the case of photons [24–26]. We have written the computer codes to implement the multiple scattering method for the calculation of the band structures of three-dimensional photonic crystals that consist of biaxial dielectric spheres. The program works efficiently and offers reliable results, which

*Electronic address: 041019018@fudan.edu.cn
†Electronic address: phlin@fudan.ac.cn

can be proved by comparing with the previous ones [10,11]. In our calculations, the maximal angular momentum is chosen as $n_c=7$, which guarantees a very good convergence of the solutions.

It is well known that for an isotropic dielectric sphere, the scattering matrix can be obtained analytically by using the Mie theory, whereas for dielectric sphere with anisotropy, it is believed that the exact scattering matrix cannot be acquired [10]. However, it is not always the case, for dielectric sphere with biaxial anisotropy, we have obtained the scattering matrix exactly within the framework of the extended Mie theory. With the scattering matrix of a single dielectric sphere obtained, by using multiple scattering method, the photonic band structure can be calculated.

The rest of our paper is organized as follows. In Sec. II, the theoretical framework of calculating scattering matrix of a single biaxial dielectric sphere is presented. At the end of Sec. II, the scattering coefficients of the whole system are provided; their static forms can be used to calculate the band structures. In Sec. III, the numerical results of the band structures of fcc and sc lattice are demonstrated. In addition, the numerical results of gap-to-midgap ratio for fcc lattice are presented. A summary is given in Sec. IV. Finally, in Appendix A some properties of vector spherical wave functions are provided, and some technical results are offered as well in Appendix B.

II. GENERAL FORMULATION

We start in Sec. II A by constructing for the electric displacement $\mathbf{D}_I$ inside the biaxial sphere a new type of vector basis functions, each of which is the solution of the wave equation for $\mathbf{D}_I$ and expanded in terms of the usual vector spherical wave functions (VSWFs) with the values of the wave vector k_l as the eigenvalues of an eigensystem determined by permittivity tensor. The electric and magnetic fields are then written as sums of the VSWFs with the different values of k_l. After expanding the incident and scattered fields in terms of VSWFs in the isotropic medium outside the sphere in Sec. II B, we match the boundary conditions to obtain, for the expansion coefficients, a linear set of coupled equations in Sec. II C, with which the scattering matrix for the biaxial sphere can be given.

A. Expansion of electromagnetic field inside sphere

The Maxwell equations for time-harmonic field inside sphere read (assuming time dependence $e^{-i\omega t}$),

$$\nabla \times \mathbf{E}_I = i\omega\mu_s \mathbf{H}_I, \tag{1a}$$

$$\nabla \times \mathbf{H}_I = -i\omega\epsilon_s \hat{\epsilon} \cdot \mathbf{E}_I, \tag{1b}$$

$$\nabla \cdot \mathbf{D}_I = 0, \tag{1c}$$

$$\nabla \cdot \mathbf{B}_I = 0. \tag{1d}$$

The constitutive relations are

$$\mathbf{B}_I = \mu_s \mathbf{H}_I, \quad \mathbf{D}_I = \epsilon_s \hat{\epsilon} \cdot \mathbf{E}_I, \tag{2}$$

where $\epsilon_s\hat{\epsilon}$ is a permittivity tensor for the biaxial sphere, given by

$$\epsilon_s\hat{\epsilon} = \epsilon_s \begin{pmatrix} \epsilon_1 & 0 & 0 \\ 0 & \epsilon_2 & 0 \\ 0 & 0 & \epsilon_3 \end{pmatrix}, \quad \hat{\epsilon}^{-1} = \begin{pmatrix} \epsilon_1' & 0 & 0 \\ 0 & \epsilon_2' & 0 \\ 0 & 0 & \epsilon_3' \end{pmatrix}, \tag{3}$$

with

$$\epsilon_1' = 1/\epsilon_1, \quad \epsilon_2' = 1/\epsilon_2, \quad \epsilon_3' = 1/\epsilon_3, \tag{4}$$

while μ_s denotes scalar permeability of the sphere. It follows from (1) and (2) that the electric displacement $\mathbf{D}_I$ satisfies

$$\nabla \times \nabla \times (\hat{\epsilon}^{-1} \cdot \mathbf{D}_I) - k_s^2 \mathbf{D}_I = 0, \tag{5}$$

with $k_s^2 = \omega^2 \epsilon_s \mu_s$. Due to $\nabla \cdot \mathbf{D}_I = 0$, $\mathbf{D}_I$ field can be expanded in terms of VSWFs as

$$\mathbf{D}_I = \sum_{n,m} \bar{E}_{mn} [c_{mn} \mathbf{M}_{mn}^{(1)}(k,\mathbf{r}) + d_{mn} \mathbf{N}_{mn}^{(1)}(k,\mathbf{r})], \tag{6}$$

where k is as yet undetermined. In general, there are three kinds of VSWFs—$\mathbf{M}_{mn}^{(J)}(k,\mathbf{r})$, $\mathbf{N}_{mn}^{(J)}(k,\mathbf{r})$, and $\mathbf{L}_{mn}^{(J)}(k,\mathbf{r})$—where $J=1$ and 3 correspond to two kinds of spherical Bessel functions [27–31]. The explicit expressions and some properties of VSWFs are given in Appendix A. The divergenceless property of $\mathbf{D}$ implies that it does not involve $\mathbf{L}_{mn}^{(J)}(k,\mathbf{r})$, thereby simplifying the algebra. Except otherwise explicitly specified, hereinafter the summation $\Sigma_{n,m}$ implies that n runs from 1 to $+\infty$ and m from $-n$ to $+n$ for each n. The implication of $\Sigma_{v,u}$ is similar. The prefactor E_{mn} is given by [27–29]

$$\bar{E}_{mn} = i^n E_0 \left[\frac{2n+1}{n(n+1)} \frac{(n-m)!}{(n+m)!} \right]^{1/2}, \tag{7}$$

where E_0 characterizes the amplitude of electric field of the incident wave. With the use of the properties of VSWFs, it can be worked out that

$$\hat{\epsilon}^{-1} \cdot \mathbf{M}_{mn} = \sum_{v=0}^{+\infty} \sum_{u=-v}^{+v} [\tilde{g}_{uv}^{mn} \mathbf{M}_{uv} + \tilde{e}_{uv}^{mn} \mathbf{N}_{uv} + \tilde{f}_{uv}^{mn} \mathbf{L}_{uv}],$$

$$\hat{\epsilon}^{-1} \cdot \mathbf{N}_{mn} = \sum_{v=0}^{+\infty} \sum_{u=-v}^{+v} [\bar{g}_{uv}^{mn} \mathbf{M}_{uv} + \bar{e}_{uv}^{mn} \mathbf{N}_{uv} + \bar{f}_{uv}^{mn} \mathbf{L}_{uv}], \tag{8}$$

where the coefficients $\tilde{g}$, $\tilde{e}$, $\tilde{f}$ and $\bar{g}$, $\bar{e}$, $\bar{f}$ are given in Appendix B. Therefore, one has

$$\hat{\epsilon}^{-1} \cdot \mathbf{D} = \sum_{n,m} \bar{E}_{mn} [\bar{c}_{mn} \mathbf{M}_{mn}^{(1)}(k,\mathbf{r}) + \bar{d}_{mn} \mathbf{N}_{mn}^{(1)}(k,\mathbf{r}) + w_{mn} \mathbf{L}_{mn}^{(1)}(k,\mathbf{r})] + w_{00} \mathbf{L}_{00}^{(1)}(k,\mathbf{r}), \tag{9}$$

where

$$\bar{c}_{mn} = \sum_{v,u} \frac{\bar{E}_{uv}}{\bar{E}_{mn}} [\tilde{g}_{mn}^{uv} c_{uv} + \bar{g}_{mn}^{uv} d_{uv}], \tag{10a}$$

$$\bar{d}_{mn} = \sum_{v,u} \frac{\bar{E}_{uv}}{\bar{E}_{mn}} [\tilde{e}^{uv}_{mn} c_{uv} + \bar{e}^{uv}_{mn} d_{uv}], \tag{10b}$$

$$w_{mn} = \sum_{v,u} \frac{\bar{E}_{uv}}{\bar{E}_{mn}} [\tilde{f}^{uv}_{mn} c_{uv} + \bar{f}^{uv}_{mn} d_{uv}], \tag{10c}$$

$$w_{00} = \frac{1}{2\sqrt{5}} \epsilon'_d d_{-22} - \frac{1}{\sqrt{30}} \epsilon'_c d_{02} + \frac{1}{2\sqrt{5}} \epsilon'_d d_{22}. \tag{10d}$$

Inserting (6) and (9) into (5), and noticing the following equations satisfied by the VSWFs:

$$\nabla \times \nabla \times \mathbf{M}^{(J)}_{mn} - k^2 \mathbf{M}^{(J)}_{mn} = 0, \tag{11a}$$

$$\nabla \times \nabla \times \mathbf{N}^{(J)}_{mn} - k^2 \mathbf{N}^{(J)}_{mn} = 0, \tag{11b}$$

$$\nabla \times \mathbf{L}^{(J)}_{mn} = 0, \tag{11c}$$

one gets

$$k^2 \sum_{n,m} \bar{E}_{mn} [\bar{c}_{mn} \mathbf{M}^{(1)}_{mn}(k,\mathbf{r}) + \bar{d}_{mn} \mathbf{N}^{(1)}_{mn}(k,\mathbf{r})] = k_s^2 \sum_{n,m} \bar{E}_{mn} [c_{mn} \mathbf{M}^{(1)}_{mn}(k,\mathbf{r}) + d_{mn} \mathbf{N}^{(1)}_{mn}(k,\mathbf{r})]. \tag{12}$$

With the use of (10), Eq. (12) becomes

$$\sum_{n,m} \bar{E}_{mn} [\tilde{c}_{mn} \mathbf{M}^{(1)}_{mn}(k,\mathbf{r}) + \tilde{d}_{mn} \mathbf{N}^{(1)}_{mn}(k,\mathbf{r})] = 0, \tag{13}$$

suggesting that

$$\tilde{d}_{mn} = k^2 \sum_{v,u} \frac{\bar{E}_{uv}}{\bar{E}_{mn}} [\bar{e}^{uv}_{mn} d_{uv} + \tilde{e}^{uv}_{mn} c_{uv}] - k_s^2 d_{mn} = 0,$$

$$\tilde{c}_{mn} = k^2 \sum_{v,u} \frac{\bar{E}_{uv}}{\bar{E}_{mn}} [\bar{g}^{uv}_{mn} d_{uv} + \tilde{g}^{uv}_{mn} c_{uv}] - k_s^2 c_{mn} = 0,$$

or, in matrix form, with $\bar{k}^2 = k^2/k_s^2$ and $\lambda = 1/\bar{k}^2$,

$$\begin{pmatrix} \bar{\mathcal{E}} & \tilde{\mathcal{E}} \\ \bar{\mathcal{G}} & \tilde{\mathcal{G}} \end{pmatrix} \begin{pmatrix} d \\ c \end{pmatrix} = \lambda \begin{pmatrix} d \\ c \end{pmatrix}, \tag{14}$$

where the matrices $\tilde{\mathcal{G}}$, $\bar{\mathcal{G}}$, $\tilde{\mathcal{E}}$ and $\bar{\mathcal{E}}$ are given by

$$\tilde{\mathcal{G}}_{mn,uv} = \frac{\bar{E}_{uv}}{\bar{E}_{mn}} \tilde{g}^{uv}_{mn}, \quad \bar{\mathcal{G}}_{mn,uv} = \frac{\bar{E}_{uv}}{\bar{E}_{mn}} \bar{g}^{uv}_{mn}, \tag{15a}$$

$$\tilde{\mathcal{E}}_{mn,uv} = \frac{\bar{E}_{uv}}{\bar{E}_{mn}} \tilde{e}^{uv}_{mn}, \quad \bar{\mathcal{E}}_{mn,uv} = \frac{\bar{E}_{uv}}{\bar{E}_{mn}} \bar{e}^{uv}_{mn}, \tag{15b}$$

with mn and uv denoting the row and column indices, respectively. Equation (14) is actually an eigensystem, with eigenvalues λ_l and eigenvectors $(d_{mn,l}, c_{mn,l})^T$. Herein, l denotes the index of eigenvalues and corresponding eigenvectors. By constructing a new vector function $\mathbf{V}_l$ based on each eigenvector,

$$\mathbf{V}_l = -\frac{i\epsilon_s}{\lambda_l} \sum_{n,m} \bar{E}_{mn} [c_{mn,l} \mathbf{M}^{(1)}_{mn}(k_l,\mathbf{r}) + d_{mn,l} \mathbf{N}^{(1)}_{mn}(k_l,\mathbf{r})], \tag{16}$$

with $k_l = \bar{k}_l k_s = k_s/\sqrt{\lambda_l}$, it is easy to show that $\mathbf{V}_l$ satisfies

$$\nabla \cdot \mathbf{V}_l = 0, \quad \nabla \times \nabla \times (\hat{\epsilon}^{-1} \cdot \mathbf{V}_l) - k_s^2 \mathbf{V}_l = 0. \tag{17}$$

Thus, the $\mathbf{D}_I$ inside the sphere can be expanded in terms of $\mathbf{V}_l$, namely,

$$\mathbf{D}_I = \sum_l \alpha_l \mathbf{V}_l. \tag{18}$$

where the expansion coefficients α_l are to be determined by matching the boundary conditions at the surface of the dielectric sphere. With $\mathbf{D}_I$ given by (18), it follows from Eqs. (2) and (1b) [noticing also Eqs. (8) and (14)] that $\mathbf{E}_I$ and $\mathbf{H}_I$ fields can be written as

$$\mathbf{E}_I = -\sum_{n,m} i\bar{E}_{mn} \sum_l \alpha_l \left[c_{mn,l} \mathbf{M}^{(1)}_{mn}(k_l,\mathbf{r}) + d_{mn,l} \mathbf{N}^{(1)}_{mn}(k_l,\mathbf{r}) + \frac{w_{mn,l}}{\lambda_l} \mathbf{L}^{(1)}_{mn}(k_l,\mathbf{r}) \right] + \sum_l i\alpha_l \left[\frac{w_{00,l}}{\lambda_l} \mathbf{L}^{(1)}_{00}(k_l,\mathbf{r}) \right], \tag{19a}$$

$$\mathbf{H}_I = \frac{-i}{\omega\mu_s} \nabla \times \mathbf{E}_I = -\frac{1}{\omega\mu_s} \sum_{n,m} \bar{E}_{mn} \sum_l k_l \alpha_l [d_{mn,l} \mathbf{M}^{(1)}_{mn}(k_l,\mathbf{r}) + c_{mn,l} \mathbf{N}^{(1)}_{mn}(k_l,\mathbf{r})], \tag{19b}$$

with

$$w_{mn,l} = \sum_{v,u} \frac{\bar{E}_{uv}}{\bar{E}_{mn}} [\bar{f}^{uv}_{mn} d_{uv,l} + \tilde{f}^{uv}_{mn} c_{uv,l}], \tag{20a}$$

$$w_{00,l} = \frac{1}{2\sqrt{5}} \epsilon'_d d_{-22,l} - \frac{1}{\sqrt{30}} \epsilon'_c d_{02,l} + \frac{1}{2\sqrt{5}} \epsilon'_d d_{22,l}. \tag{20b}$$

Since $\mathbf{E}_I$ possesses the nonzero divergence, it's expansion includes $\mathbf{L}_{mn}$, which are absent in the isotropic case.

B. Expansion of the scattered and incident fields

The scattered fields $\mathbf{E}_s$, $\mathbf{H}_s$ in the isotropic surrounding medium bear an analogy with those in Mie solution [31,32]; hence, $\mathbf{E}_s$, $\mathbf{H}_s$ along with the incident field $\mathbf{E}_{inc}$, $\mathbf{H}_{inc}$ outside the dielectric sphere are, respectively,

$$\mathbf{E}_s = \sum_{n,m} iE_{mn} [a_{mn} \mathbf{N}^{(3)}_{mn}(k_0,\mathbf{r}) + b_{mn} \mathbf{M}^{(3)}_{mn}(k_0,\mathbf{r})], \tag{21a}$$

$$\mathbf{H}_s = \frac{k_0}{\omega\mu_0} \sum_{n,m} E_{mn} [b_{mn} \mathbf{N}^{(3)}_{mn}(k_0,\mathbf{r}) + a_{mn} \mathbf{M}^{(3)}_{mn}(k_0,\mathbf{r})], \tag{21b}$$

$$\mathbf{E}_{inc} = -\sum_{n,m} iE_{mn} [p_{mn} \mathbf{N}^{(1)}_{mn}(k_0,\mathbf{r}) + q_{mn} \mathbf{M}^{(1)}_{mn}(k_0,\mathbf{r})], \tag{22a}$$

$$\mathbf{H}_{inc} = -\frac{k_0}{\omega\mu_0}\sum_{n,m} E_{mn}[q_{mn}\mathbf{N}_{mn}^{(1)}(k_0,\mathbf{r}) + p_{mn}\mathbf{M}_{mn}^{(1)}(k_0,\mathbf{r})], \tag{22b}$$

where $k_0^2=\omega^2\epsilon_0\mu_0$ with ϵ_0 and μ_0 being, respectively, the permittivity and permeability of the medium outside the sphere. The coefficients p_{mn}, q_{mn} of the incident wave and the details on their deduction can be found in Refs. [12,27].

C. Matching boundary conditions

With the internal fields, scattered fields and incident fields given in terms of the usual VSWFs, one can apply the standard boundary conditions

$$[\mathbf{E}_{inc} + \mathbf{E}_s] \times \mathbf{e}_r = \mathbf{E}_I \times \mathbf{e}_r, \tag{23a}$$

$$[\mathbf{H}_{inc} + \mathbf{H}_s] \times \mathbf{e}_r = \mathbf{H}_I \times \mathbf{e}_r, \tag{23b}$$

at the surface of sphere, which result in

$$\frac{1}{m_s}\sum_l \frac{1}{\bar{k}_l\lambda_l} j_n(\bar{k}_l m_s x) w_{mn,l}\alpha_l + \xi_n'(x)a_{mn} + \frac{1}{m_s}\sum_l \frac{1}{\bar{k}_l}\psi_n'(\bar{k}_l m_s x) d_{mn,l}\alpha_l = \psi_n'(x)p_{mn}, \tag{24a}$$

$$\xi_n(x)b_{mn} + \frac{1}{m_s}\sum_l \frac{1}{\bar{k}_l}\psi_n(\bar{k}_l m_s x) c_{mn,l}\alpha_l = \psi_n(x)q_{mn}, \tag{24b}$$

$$\xi_n(x)a_{mn} + \frac{\mu_0}{\mu_s}\sum_l \psi_n(\bar{k}_l m_s x) d_{mn,l}\alpha_l = \psi_n(x)p_{mn}, \tag{24c}$$

$$\xi_n'(x)b_{mn} + \frac{\mu_0}{\mu_s}\sum_l \psi_n'(\bar{k}_l m_s x) c_{mn,l}\alpha_l = \psi_n'(x)q_{mn}, \tag{24d}$$

where

$$x = k_0 r_s, \quad m_s = \frac{k_s}{k_0}, \quad \bar{k}_l = \frac{k_l}{k_s},$$

$$k_l = m_s\bar{k}_l k_0, \quad \lambda_l = \frac{k_s^2}{k_l^2} = \frac{1}{\bar{k}_l^2}, \tag{25}$$

with r_s the radius of sphere. The Ricatti-Bessel functions $\psi_n(z)$, $\xi_n(z)$ are given by [32]

$$\psi_n(z) = zj_n(z), \quad \xi_n(z) = zh_n^{(1)}(z). \tag{26}$$

Equation (24) can be rewritten as

$$p_{mn} = \left[\frac{\xi_n'(x)}{\psi_n'(x)}\right]a_{mn} + \sum_l \left[\frac{1}{m_s\bar{k}_l}\frac{\psi_n'(\bar{k}_l m_s x)}{\psi_n'(x)} d_{mn,l}\right]\alpha_l + \sum_l \left[\frac{1}{m_s\bar{k}_l\lambda_l}\frac{j_n(\bar{k}_l m_s x)}{\psi_n'(x)} w_{mn,l}\right]\alpha_l, \tag{27a}$$

$$q_{mn} = \left[\frac{\xi_n(x)}{\psi_n(x)}\right]b_{mn} + \sum_l \left[\frac{1}{m_s\bar{k}_l}\frac{\psi_n(\bar{k}_l m_s x)}{\psi_n(x)} c_{mn,l}\right]\alpha_l, \tag{27b}$$

$$p_{mn} = \left[\frac{\xi_n(x)}{\psi_n(x)}\right]a_{mn} + \sum_l \left[\frac{\mu_0}{\mu_s}\frac{\psi_n(\bar{k}_l m_s x)}{\psi_n(x)} d_{mn,l}\right]\alpha_l, \tag{27c}$$

$$q_{mn} = \left[\frac{\xi_n'(x)}{\psi_n'(x)}\right]b_{mn} + \sum_l \left[\frac{\mu_0}{\mu_s}\frac{\psi_n'(\bar{k}_l m_s x)}{\psi_n'(x)} c_{mn,l}\right]\alpha_l. \tag{27d}$$

In matrix form

$$\begin{pmatrix} W \\ 0 \end{pmatrix}\tilde{\alpha} + \begin{pmatrix} \Lambda' & 0 \\ 0 & \Lambda \end{pmatrix}\begin{pmatrix} a \\ b \end{pmatrix} + \begin{pmatrix} U' \\ U \end{pmatrix}\tilde{\alpha} = \begin{pmatrix} p \\ q \end{pmatrix}, \tag{28a}$$

$$\begin{pmatrix} \Lambda & 0 \\ 0 & \Lambda' \end{pmatrix}\begin{pmatrix} a \\ b \end{pmatrix} + \begin{pmatrix} V \\ V' \end{pmatrix}\tilde{\alpha} = \begin{pmatrix} p \\ q \end{pmatrix}, \tag{28b}$$

where Λ and Λ' are $n_d\times n_d$ diagonal matrices, U, U', V, V', and W are $n_d\times 2n_d$ matrices, while $\tilde{\alpha}$ a $2n_d\times 1$ matrix. Here $n_d=n_c(n_c+2)$ with n_c the maximum angular momentum. Explicitly,

$$W_{mn,l} = \frac{1}{m_s^2 x}\frac{\bar{T}_n(x,m_s\bar{k}_l x)}{D_n^{(1)}(m_s\bar{k}_l x)} w_{mn,l},$$

$$\Lambda_{mn,uv} = S_n(x)\delta_{nv}\delta_{mu},$$

$$\Lambda'_{mn,uv} = \bar{S}_n(x)\delta_{nv}\delta_{mu},$$

$$U_{mn,l} = \frac{1}{m_s\bar{k}_l} T_n(x,m_s\bar{k}_l x) c_{mn,l},$$

$$U'_{mn,l} = \frac{1}{m_s\bar{k}_l}\bar{T}_n(x,m_s\bar{k}_l x) d_{mn,l},$$

$$V_{mn,l} = \frac{\mu_0}{\mu_s} T_n(x,m_s\bar{k}_l x) d_{mn,l},$$

$$V'_{mn,l} = \frac{\mu_0}{\mu_s}\bar{T}_n(x,m_s\bar{k}_l x) c_{mn,l}, \tag{29}$$

where

$$S_n(x) = \frac{\xi_n(x)}{\psi_n(x)}, \quad \bar{S}_n(x) = \frac{\xi_n'(x)}{\psi_n'(x)},$$

$$T_n(x,z) = \frac{\psi_n(z)}{\psi_n(x)}, \quad \bar{T}_n(x,z) = \frac{\psi_n'(z)}{\psi_n'(x)}, \quad D_n^{(1)}(z) = \frac{\psi_n'(z)}{\psi_n(z)}.$$

Equations (28a) and (28b) can be solved to give

$$\begin{pmatrix} a \\ b \end{pmatrix} = \mathcal{S}\begin{pmatrix} p \\ q \end{pmatrix} = \mathcal{Z}\mathcal{R}\begin{pmatrix} p \\ q \end{pmatrix}, \quad \tilde{\alpha} = \mathcal{R}\begin{pmatrix} p \\ q \end{pmatrix}, \tag{30}$$

where

$$\mathcal{R} = \left[\begin{pmatrix} U' + W \\ U \end{pmatrix} + \begin{pmatrix} \Lambda' & 0 \\ 0 & \Lambda \end{pmatrix} \mathcal{Z} \right]^{-1}, \tag{31}$$

$$\mathcal{Z} = \begin{pmatrix} \Lambda' - \Lambda & 0 \\ 0 & \Lambda - \Lambda' \end{pmatrix}^{-1} \begin{pmatrix} V - U' - W \\ V' - U \end{pmatrix}. \tag{32}$$

With the scattering matrix $\mathcal{S}$ for a single sphere known, the scattering coefficients of sphere j for multiple spheres scattering can be written as

$$\begin{pmatrix} a^{(j)} \\ b^{(j)} \end{pmatrix} = \mathcal{S}^{(j)} \left[\begin{pmatrix} p^{(j,j)} \\ q^{(j,j)} \end{pmatrix} - \sum_{l \neq j} \begin{pmatrix} a^{(l)} & b^{(l)} \\ b^{(l)} & a^{(l)} \end{pmatrix} \begin{pmatrix} A(l,j) \\ B(l,j) \end{pmatrix} \right] \tag{33}$$

where $\mathcal{S}^{(j)}$ corresponds to the scattering matrix of single sphere j as given in Eq. (30), $p^{(j,j)}$ and $q^{(j,j)}$ correspond to the expansion coefficients of the incident wave on sphere j, $a^{(l)}$ and $b^{(l)}$ correspond to the expansion coefficients of sphere l expanded around sphere l, $A(l,j)$ and $B(l,j)$ are vector translational coefficients that translate the scattering coefficients expanded around sphere l into those around sphere j. The above results can be applied to special lattice structures to calculate the photonic band structures, and for this purpose only the stationary-state solution should be concerned, i.e., $p_{mn}^{j,j} = q_{mn}^{j,j} = 0$.

III. RESULTS AND DISCUSSION

In present work, we take $\epsilon_s = 35$, $\epsilon_3 = 1.0$, while ϵ_1, ϵ_2 can be modulated to find appropriate values. For convenience but without loss of generality, we take air as background medium. As has been demonstrated in a previous paper, for the lattice consisting of uniaxially birefringent dielectric spheres, if the extraordinary axis is along the [111] direction, the complete PBGs appear in simple lattice structures such as fcc and sc [11]. Therefore, in our calculation of PBGs, the extraordinary axis is chosen as principle axis ϵ_3 with the fixed value $\epsilon_3 = 1.0$, and its orientation is also oriented along [111] direction, while the two ordinary axes ϵ_1 and ϵ_2 are along $[11\bar{2}]$ and $[\bar{1}10]$ directions, respectively. This orientation is obtained through rotating the conventional crystallographic orientation with ϵ_1, ϵ_2, and ϵ_3 in x, y, and z directions, respectively, by Euler angles $\left(\frac{\pi}{4}, \arccos\frac{1}{\sqrt{3}}, 0\right)$. In calculating the band structure of photonic crystals consisting of isotropic dielectric spheres, only 1/48th of the first Brillouin zone is concerned because of the symmetry. However, herein with the existence of the anisotropy most of the symmetries break down, the only one kept is the inverse symmetry, which means that the points (a,b,c) and $(-a,-b,-c)$ are equivalent. To that extent, the calculation of the band structure should be performed over one-half of the whole Brillouin zone. In the calculation of band structure of photonic crystals composed of birefringent dielectric spheres, an alternative and equivalent method is employed, i.e., investigating the band structure along the symmetry lines in a fixed region of the first Brillouin zone, while transforming the dielectric constant dyadic in real space [17]. In our case the situation is much more complicated, which may lead to the confusion if we employ the above method, so herein we calculate the band structures along the boundaries of 24 different 1/48th partial regions of the first Brillouin zone directly while fixing the crystallographic orientations of ϵ_1, ϵ_2, and ϵ_3 (which are always in directions $[11\bar{2}]$, $[\bar{1}10]$, and [111], respectively).

Compared with birefringent case, the biaxial anisotropy enhances the anisotropy, which results in more lifting of degeneracy, thus giving rise to the further split of the photonic band structure, then we can expect the appearance of new PBGs or enlargement of PBG. The calculated photonic band structures for the fcc lattice consisting of dielectric spheres in air with filling fraction $f = 0.25$ and permittivities $\epsilon_s = 35$, $\epsilon_1 = 0.65$, $\epsilon_2 = 0.75$, $\epsilon_3 = 1.0$ are shown in Fig. 1. In our calculation 24 partial regions of the first Brillouin zone are considered. Shown in Fig. 1 are eight band structures that correspond to eight partial regions of the first Brillouin zone. The high symmetry points in the band structures are (a) $\Gamma = (0,0,0)$, $X = (2\pi/a)(0,1,0)$, $U = (2\pi/a)\left(\frac{1}{4},1,\frac{1}{4}\right)$, $L = (2\pi/a)\left(\frac{1}{2},\frac{1}{2},\frac{1}{2}\right)$, $W = (2\pi/a)\left(\frac{1}{2},1,0\right)$, $K = (2\pi/a)\left(\frac{3}{4},\frac{3}{4},0\right)$; (b) the same as (a) except $W = (2\pi/a)\left(0,1,\frac{1}{2}\right)$, $K = (2\pi/a) \times \left(0,\frac{3}{4},\frac{3}{4}\right)$; (c) $\Gamma = (0,0,0)$, $X = (2\pi/a)(0,0,1)$, $U = (2\pi/a) \times \left(\frac{1}{4},\frac{1}{4},1\right)$, $L = (2\pi/a)\left(\frac{1}{2},\frac{1}{2},\frac{1}{2}\right)$, $W = (2\pi/a)\left(0,\frac{1}{2},1\right)$, $K = (2\pi/a)\left(0,\frac{3}{4},\frac{3}{4}\right)$; (d) the same as (c) except $W = (2\pi/a) \times \left(\frac{1}{2},0,1\right)$, $K = (2\pi/a)\left(\frac{3}{4},0,\frac{3}{4}\right)$; (e) $\Gamma = (0,0,0)$, $X = (2\pi/a) \times (0,0,-1)$, $U = (2\pi/a)\left(\frac{1}{4},\frac{1}{4},-1\right)$, $L = (2\pi/a)\left(\frac{1}{2},\frac{1}{2},-\frac{1}{2}\right)$, $W = (2\pi/a)\left(0,\frac{1}{2},-1\right)$, $K = (2\pi/a)\left(0,\frac{3}{4},-\frac{3}{4}\right)$; (f) the same as (e) except $W = (2\pi/a)\left(\frac{1}{2},0,-1\right)$, $K = (2\pi/a)\left(\frac{3}{4},0,-\frac{3}{4}\right)$; (g) $\Gamma = (0,0,0)$, $X = (2\pi/a)(1,0,0)$, $U = (2\pi/a)\left(1,\frac{1}{4},-\frac{1}{4}\right)$, $L = (2\pi/a)\left(\frac{1}{2},\frac{1}{2},-\frac{1}{2}\right)$, $W = (2\pi/a)\left(1,0,-\frac{1}{2}\right)$, $K = (2\pi/a)\left(\frac{3}{4},0,-\frac{3}{4}\right)$; (h) the same as (g) except $W = (2\pi/a)\left(1,\frac{1}{2},0\right)$, $K = (2\pi/a)\left(\frac{3}{4},\frac{3}{4},0\right)$. It is clearly seen from the eight diagrams in Fig. 1 that a common PBG exists between the second and third photonic bands. The same PBG appears also in the remaining 16 partial band structures. We note that due to the anisotropy, the extremes of the bands may deviate away from the boundary of the Brillouin zone, leading to the closing of the PBG at nonboundary k-points. To check this, we have calculate the eigenfrequencies of some k-points off the Brillouin zone boundaries, our results show no eigenfrequencies appear in the gap frequency range. Although this does not serve as a rigorous proof, we believe our results render a possibility to obtain the complete PBGs through introducing the anisotropy. In addition to the complete PBG, a neighboring partial PBG, as shown in Figs. 1(e)–1(h), exists between the third and fourth bands that is absent in the birefringent case. The partial gap arises from the enhancement of the anisotropy since the third and the fourth bands degenerate at the Γ-point in the birefringent case [11].

As has been shown in previous results, the filling fraction of dielectric spheres is an important factor to determine the complete PBGs. In Fig. 2, we show the complete bandgap-to-midgap ratio as a function of the filling fraction. It can be seen from the diagram that the gap-to-midgap ratio increases sharply with the filling fraction f when it is less than 0.23. At $f = 0.25$, the gap-to-midgap ratio reaches its maximal value of about 2.5%; then, the gap-to-midgap ratio keeps a relatively

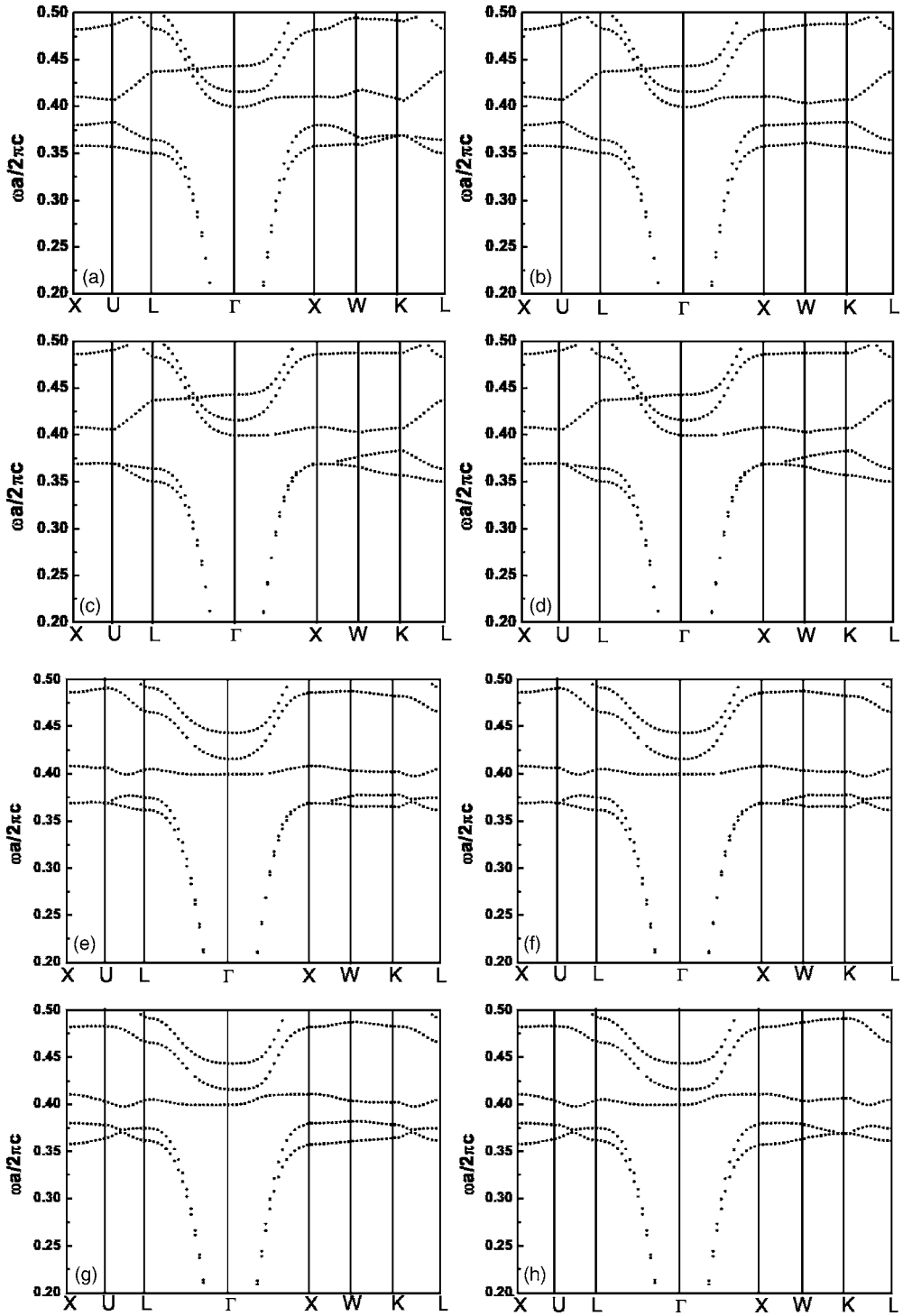

FIG. 1. Calculated photonic band structures of a PC consisting of biaxial dielectric spheres in fcc lattice with permittivity tensor $\epsilon_s=35$, $\epsilon_1=0.65$, $\epsilon_2=0.75$, $\epsilon_3=1.0$. The extraordinary axis, corresponding to the principal axis ϵ_3 with $\epsilon_3=1.0$, is oriented along the [111] direction and the two ordinary axes ϵ_1 and ϵ_2 are along the $[11\bar{2}]$ and $[\bar{1}10]$ directions, respectively. The filling fraction is $f=0.25$. The photonic band structures of this PC in 24 partial regions (one-half of the first Brillouin zone) are calculated. The above eight diagrams correspond to eight partial regions respectively in the first Brillouin zone with the high symmetry points: (a) $\Gamma=(0,0,0)$, $X=(2\pi/a)\times(0,1,0)$, $U=(2\pi/a)(\frac{1}{4},1,\frac{1}{4})$, $L=(2\pi/a)(\frac{1}{2},\frac{1}{2},\frac{1}{2})$, $W=(2\pi/a)(\frac{1}{2},1,0)$, $K=(2\pi/a)(\frac{3}{4},\frac{3}{4},0)$; (b) the same as (a) except $W=(2\pi/a)(0,1,\frac{1}{2})$, $K=(2\pi/a)(0,\frac{3}{4},\frac{3}{4})$; (c) $\Gamma=(0,0,0)$, $X=(2\pi/a)(0,0,1)$, $U=(2\pi/a)(\frac{1}{4},\frac{1}{4},1)$, $L=(2\pi/a)(\frac{1}{2},\frac{1}{2},\frac{1}{2})$, $W=(2\pi/a)(0,\frac{1}{2},1)$, $K=(2\pi/a)(0,\frac{3}{4},\frac{3}{4})$; (d) the same as (c) except $W=(2\pi/a)(\frac{1}{2},0,1)$, $K=(2\pi/a)(\frac{3}{4},0,\frac{3}{4})$; (e) $\Gamma=(0,0,0)$, $X=(2\pi/a)(0,0,-1)$, $U=(2\pi/a)(\frac{1}{4},\frac{1}{4},-1)$, $L=(2\pi/a)(\frac{1}{2},\frac{1}{2},-\frac{1}{2})$, $W=(2\pi/a)(0,\frac{1}{2},-1)$, $K=(2\pi/a)(0,\frac{3}{4},-\frac{3}{4})$; (f) the same as (e) except $W=(2\pi/a)(\frac{1}{2},0,-1)$, $K=(2\pi/a)(\frac{3}{4},0,-\frac{3}{4})$; (g) $\Gamma=(0,0,0)$, $X=(2\pi/a)(1,0,0)$, $U=(2\pi/a)(1,\frac{1}{4},-\frac{1}{4})$, $L=(2\pi/a)(\frac{1}{2},\frac{1}{2},-\frac{1}{2})$, $W=(2\pi/a)(1,0,-\frac{1}{2})$, $K=(2\pi/a)(\frac{3}{4},0,-\frac{3}{4})$; (h) the same as (g) except $W=(2\pi/a)(1,\frac{1}{2},0)$, $K=(2\pi/a)(\frac{3}{4},\frac{3}{4},0)$.

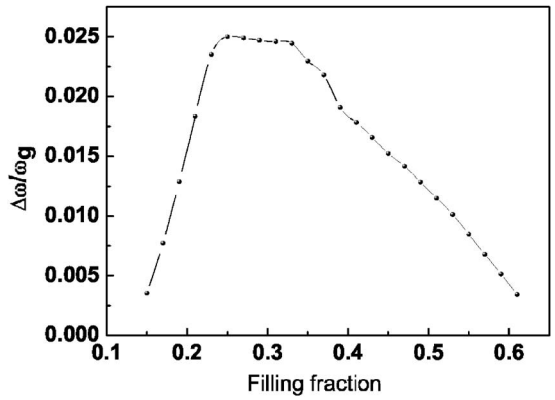

FIG. 2. The gap-to-midgap ratio of the complete band gap vs filling fraction from the PC in fcc lattice structure with $\epsilon_s=35$, $\epsilon_1=0.65$, $\epsilon_2=0.75$ and $\epsilon_3=1.0$. The extraordinary axis, corresponding to the principal axis ϵ_3 with $\epsilon_3=1.0$, is oriented along the [111] direction and the two ordinary axes ϵ_1 and ϵ_2 are along the $[11\bar{2}]$ and $[\bar{1}10]$ directions respectively.

high value until the filling fraction is close to 4.0, and after that the gap-to-midgap ratio decreases gradually with the filling ratio f. In particular, the complete PBG exists in a wide range of low filling fraction.

As for the partial gap, the values of partial-gap-to-midgap ratios corresponding to the band structures in Fig. 1(e) and Fig. 1(f) are investigated. The results are shown in Fig. 3(a) and Fig. 3(b). The shapes of the curves are almost the same, which suggests these two partial region possess the similar symmetry. We can also examine it from the band structures corresponding to the partial regions as shown in Fig. 1(e) and Fig. 1(f). For the first partial region the maximum gap-to-midgap ratio is 1.08% at $f=0.29$. For the second partial region the maximum gap to midgap ratio is 1.10% at $f=0.29$. It can be found from Fig. 3(a) and Fig. 3(b) that the above two partial PBGs are stable. However, compared with the complete PBG as shown in Fig. 2 they exist in relatively narrower range of filling fraction.

The photonic band structure of sc has also been calculated and the complete PBGs are found. As in the fcc, 24 partial regions in the first Brillouin zone are taken into account. The result is shown in Fig. 4, which corresponds to the band structures in eight partial regions. The high symmetry points in the band structures are (a) $\Gamma=(0,0,0)$, $X=(2\pi/a)\times(0,\frac{1}{2},0)$, $R=(2\pi/a)(\frac{1}{2},\frac{1}{2},\frac{1}{2})$, $M=(2\pi/a)(\frac{1}{2},\frac{1}{2},0)$; (b) the same as (a) except $M=(2\pi/a)(0,\frac{1}{2},\frac{1}{2})$; (c) $\Gamma=(0,0,0)$, $X=(2\pi/a)(0,0,\frac{1}{2})$, $R=(2\pi/a)(\frac{1}{2},\frac{1}{2},\frac{1}{2})$, $M=(2\pi/a)(0,\frac{1}{2},\frac{1}{2})$; (d) the same as (c) except $M=(2\pi/a)(\frac{1}{2},0,\frac{1}{2})$; (e) $\Gamma=(0,0,0)$, $X=(2\pi/a)(0,0,-\frac{1}{2})$, $R=(2\pi/a)(\frac{1}{2},\frac{1}{2},-\frac{1}{2})$, $M=(2\pi/a)(0,\frac{1}{2},-\frac{1}{2})$; (f) the same as (e) except $M=(2\pi/a)(\frac{1}{2},0,-\frac{1}{2})$; (g) $\Gamma=(0,0,0)$, $X=(2\pi/a)(\frac{1}{2},0,0)$, $R=(2\pi/a)(\frac{1}{2},\frac{1}{2},-\frac{1}{2})$, $M=(2\pi/a)(\frac{1}{2},0,-\frac{1}{2})$; (h) the same as (g) except $M=(2\pi/a)\times(\frac{1}{2},\frac{1}{2},0)$. The band structure is quite similar to the birefringent case, yet it offers a way to check how the anisotropy affects the photonic band structure and its degeneracy. It can be found when anisotropy (modulated through altering the values of ϵ_1, ϵ_2 and keeping $\epsilon_3=1.0$ fixed) increases the degeneracy of the photonic band structure will decrease and the split of the band structure will be enlarged, which can even lead to the close of the bandgap.

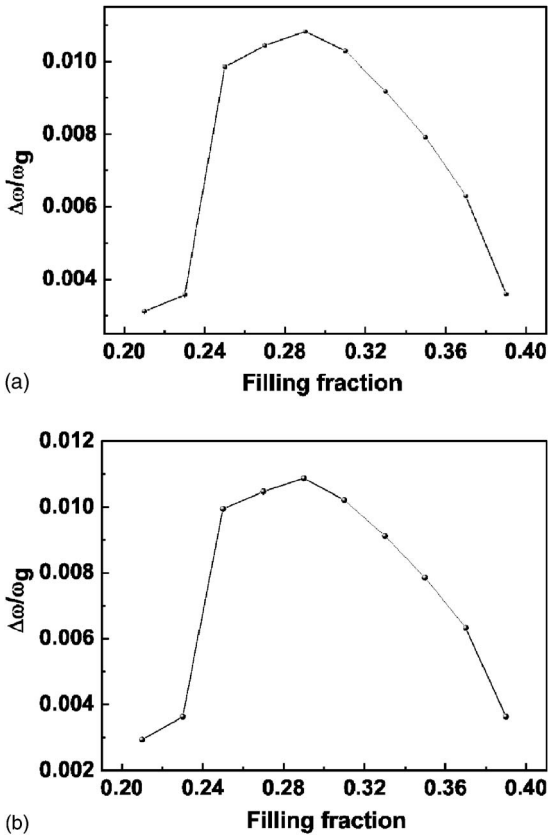

FIG. 3. The gap-to-midgap ratios of the partial PBGs as a function of filling fraction from the PC in fcc lattice structure composed of biaxial dielectric spheres with $\epsilon_s=35$, $\epsilon_1=0.65$, $\epsilon_2=0.75$, $\epsilon_3=1.0$. The extraordinary axis, corresponding to the principal axis ϵ_3 with $\epsilon_3=1.0$, is oriented along the [111] direction and the two ordinary axes ϵ_1 and ϵ_2 are along the $[11\bar{2}]$ and $[\bar{1}10]$ directions respectively. The above two diagrams correspond to two partial regions of the first Brillouin zone with high symmetry points (a) $\Gamma=(0,0,0)$, $X=(2\pi/a)(0,0,-1)$, $U=(2\pi/a)(\frac{1}{4},\frac{1}{4},-1)$, $L=(2\pi/a)(\frac{1}{2},\frac{1}{2},-\frac{1}{2})$, $W=(2\pi/a)(0,\frac{1}{2},-1)$, $K=(2\pi/a)(0,\frac{3}{4},-\frac{3}{4})$; (b) the same as (a) except $W=(2\pi/a)(\frac{1}{2},0,-1)$, $K=(2\pi/a)(\frac{3}{4},0,-\frac{3}{4})$.

The photonic band structures for the extraordinary axes are along [100] and [110] directions have also been calculated, but the results show that no complete PBGs can be found as reported in other papers [11,17]. However, along the [111] direction the complete PBGs are found, suggesting that altering the direction of extraordinary axis is also an important approach to achieve some degree of tunability of the photonic band structure.

IV. CONCLUSION

In this paper, we have extended the framework of Mie scattering theory to obtain the scattering matrix of single dielectric sphere with biaxial anisotropy. By employing the multiple scattering method, we then calculate the photonic band structures of PCs consisting of the biaxial dielectric spheres. The results demonstrate the possibility of the pres-

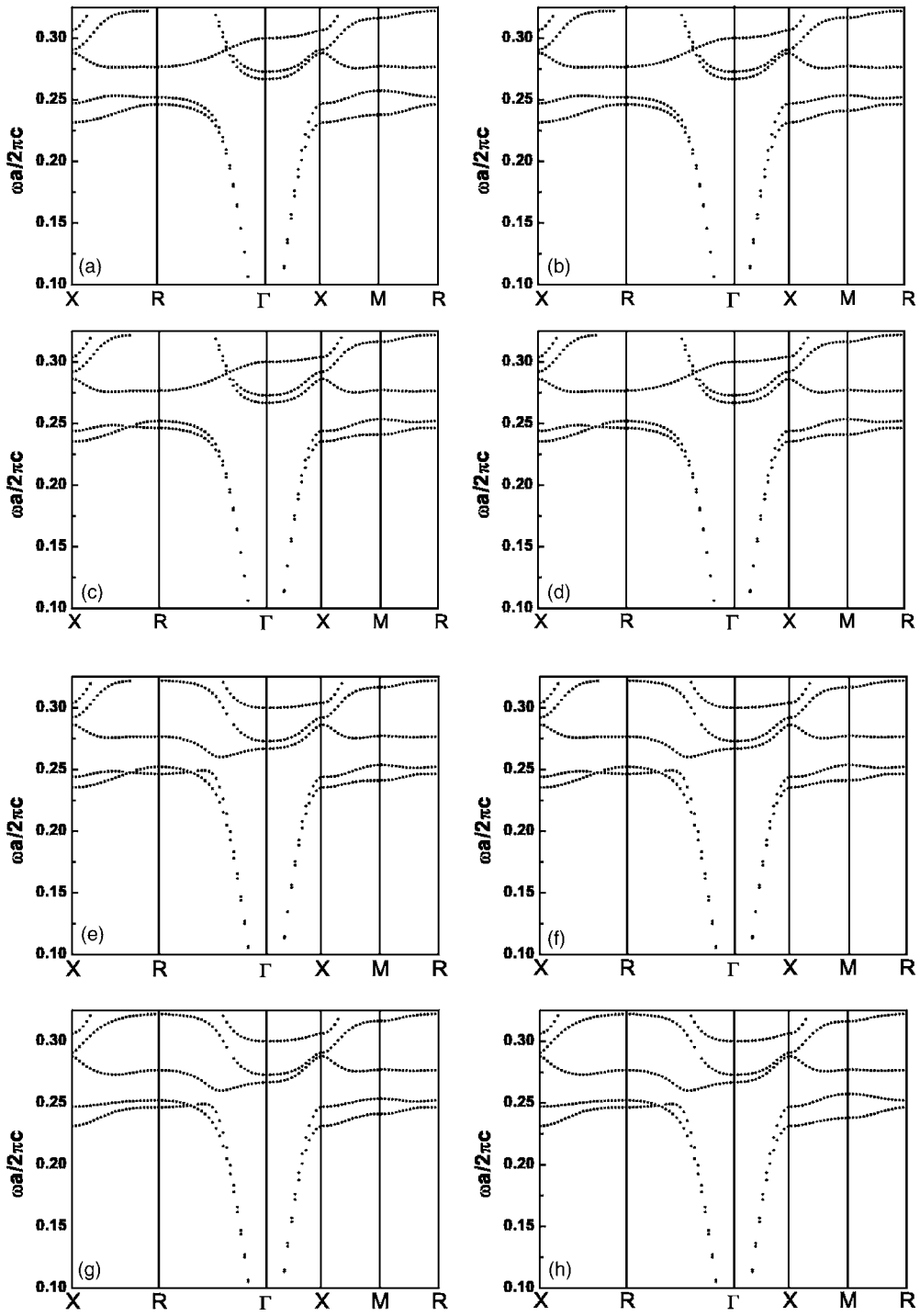

FIG. 4. Calculated photonic band structures of a PC consisting of biaxial dielectric spheres in sc lattice with permittivity tensor $\epsilon_s=35$, $\epsilon_1=0.60$, $\epsilon_2=0.65$, $\epsilon_3=1.0$. The extraordinary axis, corresponding to the principal axis ϵ_3 with $\epsilon_3=1.0$, is oriented along the [111] direction and the two ordinary axes ϵ_1 and ϵ_2 are along the $[11\bar{2}]$ and $[\bar{1}10]$ directions respectively. The filling fraction is $f=0.23$. The photonic band structures of this PC in 24 partial regions (one-half of the first Brillouin zone) are plotted. The above eight diagrams correspond to eight partial regions, respectively, in the first Brillouin zone with the high symmetry points: (a) $\Gamma=(0,0,0)$, $X=(2\pi/a)(0,\frac{1}{2},0)$, $R=(2\pi/a)\times(\frac{1}{2},\frac{1}{2},\frac{1}{2})$, $M=(2\pi/a)(\frac{1}{2},\frac{1}{2},0)$; (b) the same as (a) except $M=(2\pi/a)(0,\frac{1}{2},\frac{1}{2})$; (c) $\Gamma=(0,0,0)$, $X=(2\pi/a)(0,0,\frac{1}{2})$, $R=(2\pi/a)(\frac{1}{2},\frac{1}{2},\frac{1}{2})$, $M=(2\pi/a)(0,\frac{1}{2},\frac{1}{2})$; (d) the same as (c) except $M=(2\pi/a)(\frac{1}{2},0,\frac{1}{2})$; (e) $\Gamma=(0,0,0)$, $X=(2\pi/a)(0,0,-\frac{1}{2})$, $R=(2\pi/a)(\frac{1}{2},\frac{1}{2},-\frac{1}{2})$, $M=(2\pi/a)\times(0,\frac{1}{2},-\frac{1}{2})$; (f) the same as (e) except $M=(2\pi/a)(\frac{1}{2},0,-\frac{1}{2})$; (g) $\Gamma=(0,0,0)$, $X=(2\pi/a)(\frac{1}{2},0,0)$, $R=(2\pi/a)(\frac{1}{2},\frac{1}{2},-\frac{1}{2})$, $M=(2\pi/a)(\frac{1}{2},0,-\frac{1}{2})$; (h) the same as (g) except $M=(2\pi/a)(\frac{1}{2},\frac{1}{2},0)$.

ence of complete PBGs in fcc and sc lattice structures with extraordinary axis along the [111] direction, confirming that the direction of extraordinary axis can be an important factor to modulate the band structure. In particular, for fcc lattice structure, in addition to a complete PBGs as in the birefringent case, a neighboring partial PBG is observed in biaxial case, due to the further lifting of degeneracy in photonic band structure. Compared with birefringent case, the theoretical framework for dielectric sphere with biaxial anisotropy offers much more flexibilities to optimize the band structure, consequently, providing with much more chances in opening up and/or tuning the PBGs.

Finally, as has been mentioned, due to the anisotropy the extremes of the bands may not locate at the boundary of the Brillouin zone. Although we have calculated eigenfrequencies of k-points off the boundary of the Brillouin zone boundaries and found no eigenfrequencies in the PBG frequency range, suggesting that the PBG may be a complete one, it is not a rigorous proof as in the isotropic case. A cleaner understanding may be the calculation of density of states as a function of frequency, work along this line is in progress.

ACKNOWLEDGMENTS

This work was supported by CNKBRSF, NNSFC through Grant Nos. 10474014 and 10321003, and PCSIRT.

APPENDIX A: VECTOR SPHERICAL WAVE FUNCTIONS

The vector spherical wave functions (VSWFs) $\mathbf{M}_{mn}^{(J)}$, $\mathbf{N}_{mn}^{(J)}$, and $\mathbf{L}_{mn}^{(J)}$ are given by [27–31]

$$\begin{aligned}\mathbf{L}_{mn}^{(J)}(k,\mathbf{r}) &= \frac{1}{k}\nabla\Phi_{mn}^{(J)}(k,\mathbf{r}) \\ &= [\tau_{mn}(\cos\theta)\mathbf{e}_\theta + i\pi_{mn}(\cos\theta)\mathbf{e}_\phi] \\ &\quad\times\frac{z_n^{(J)}(kr)}{kr}\exp(im\phi) + \mathbf{e}_r P_n^m(\cos\theta) \\ &\quad\times\frac{1}{k}\frac{d}{dr}[z_n^{(J)}(kr)]\exp(im\phi),\end{aligned}$$

$$\begin{aligned}\mathbf{M}_{mn}^{(J)}(k,\mathbf{r}) &= \nabla\times[\mathbf{r}\Phi_{mn}^{(J)}(k,\mathbf{r})] \\ &= [i\pi_{mn}(\cos\theta)\mathbf{e}_\theta - \tau_{mn}(\cos\theta)\mathbf{e}_\phi] \\ &\quad\times z_n^{(J)}(kr)\exp(im\phi),\end{aligned}$$

$$\begin{aligned}\mathbf{N}_{mn}^{(J)}(k,\mathbf{r}) &= \frac{1}{k}\nabla\times\mathbf{M}_{mn}^{(J)}(k,\mathbf{r}) \\ &= [\tau_{mn}(\cos\theta)\mathbf{e}_\theta + i\pi_{mn}(\cos\theta)\mathbf{e}_\phi]\frac{1}{kr}\frac{d}{dr}[rz_n^{(J)}(kr)] \\ &\quad\times\exp(im\phi) + \mathbf{e}_r n(n+1)P_n^m(\cos\theta)\frac{z_n^{(J)}(kr)}{kr} \\ &\quad\times\exp(im\phi),\end{aligned} \tag{A1}$$

where $\mathbf{e}_r$, $\mathbf{e}_\theta$, and $\mathbf{e}_\phi$ are three unit base vectors in spherical coordinate system, and $P_n^m(x)$ is the first kind associated Legendre function [31,32]. In Eq. (A1),

$$\Phi_{mn}^{(J)}(k,\mathbf{r}) = P_n^m(\cos\theta)\exp(im\phi)z_n^{(J)}(kr), \tag{A2}$$

satisfying the scalar Helmholtz equation

$$\nabla^2\Phi_{mn}^{(J)}(k,\mathbf{r}) + k^2\Phi_{mn}^{(J)}(k,\mathbf{r}) = 0. \tag{A3}$$

The radial function $z_n^{(J)}$ is appropriately selected from the four spherical Bessel functions. In our formulae, $J=1$ and 3 correspond to the first kind spherical Bessel function and the first kind spherical Hankel function, respectively, namely,

$$z_n^{(1)}(x) = j_n(x), \quad z_n^{(3)}(x) = h_n^{(1)}(x). \tag{A4}$$

Two auxiliary functions, $\pi_{mn}(\cos\theta)$ and $\tau_{mn}(\cos\theta)$, are defined by

$$\begin{aligned}\pi_{mn}(\cos\theta) &= \frac{m}{\sin\theta}P_n^m(\cos\theta), \\ \tau_{mn}(\cos\theta) &= \frac{d}{d\theta}P_n^m(\cos\theta).\end{aligned} \tag{A5}$$

They satisfy the following relations [32]:

$$\begin{aligned}\int_0^\pi (\pi_{mn}\tau_{m\nu} + \pi_{m\nu}\tau_{mn})\sin\theta d\theta = 0, \\ \int_0^\pi (\pi_{mn}\pi_{m\nu} + \tau_{mn}\tau_{m\nu})\sin\theta d\theta = \frac{2n(n+1)}{2n+1}\frac{(n+m)!}{(n-m)!}\delta_{n\nu}.\end{aligned} \tag{A6}$$

The VSWFs satisfy

$$\begin{aligned}\nabla\times\nabla\times\mathbf{M}_{mn}^{(J)} - k^2\mathbf{M}_{mn}^{(J)} = 0, \\ \nabla\times\nabla\times\mathbf{N}_{mn}^{(J)} - k^2\mathbf{N}_{mn}^{(J)} = 0,\end{aligned} \tag{A7a}$$

$$\mathbf{M}_{mn}^{(J)} = \frac{1}{k}\nabla\times\mathbf{N}_{mn}^{(J)}, \quad \mathbf{N}_{mn}^{(J)} = \frac{1}{k}\nabla\times\mathbf{M}_{mn}^{(J)}, \tag{A7b}$$

$$\nabla\cdot\mathbf{M}_{mn}^{(J)} = 0, \quad \nabla\cdot\mathbf{N}_{mn}^{(J)} = 0, \quad \nabla\times\mathbf{L}_{mn}^{(J)} = 0. \tag{A7c}$$

The VSWFs satisfy the orthogonality in the sense that [31]

$$\int\mathbf{M}_{uv}^{\star}\cdot\mathbf{N}_{mn}d\Omega = 0, \quad \int\mathbf{L}_{uv}^{\star}\cdot\mathbf{M}_{mn}d\Omega = 0,$$

$$\int\mathbf{M}_{uv}^{\star}\cdot\mathbf{M}_{mn}d\Omega = \frac{4\pi n(n+1)}{2n+1}\frac{(n+m)!}{(n-m)!}z_n^2(kr)\delta_{mu}\delta_{n\nu},$$

$$\begin{aligned}\int\mathbf{N}_{uv}^{\star}\cdot\mathbf{N}_{mn}d\Omega = \frac{4\pi n(n+1)}{(2n+1)^2}\frac{(n+m)!}{(n-m)!}[(n+1)z_{n-1}^2(kr) \\ + nz_{n+1}^2(kr)]\delta_{mu}\delta_{n\nu},\end{aligned}$$

$$\begin{aligned}\int\mathbf{L}_{uv}^{\star}\cdot\mathbf{L}_{mn}d\Omega = \frac{4\pi}{(2n+1)^2}\frac{(n+m)!}{(n-m)!}[nz_{n-1}^2(kr) \\ + (n+1)z_{n+1}^2(kr)]\delta_{mu}\delta_{n\nu},\end{aligned}$$

$$\int \mathbf{L}_{uv}^{\star} \cdot \mathbf{N}_{mn} d\Omega = \frac{4\pi n(n+1)}{(2n+1)^2} \frac{(n+m)!}{(n-m)!} [z_{n-1}^2(kr) - z_{n+1}^2(kr)] \delta_{mu} \delta_{nv}, \tag{A8}$$

where $\star$ denotes complex conjugate on angular functions, $d\Omega$ means the integrals are performed over the entire solid angle.

APPENDIX B: THE COEFFICIENTS $\tilde{G}$, $\tilde{E}$, $\tilde{F}$, $\bar{G}$, $\bar{E}$, AND $\bar{F}$

With $\epsilon_d' = \epsilon_1' - \epsilon_2'$ and $\epsilon_c' = \epsilon_1' + \epsilon_2' - 2\epsilon_3'$,

$$\tilde{g}_{uv}^{mn} = \frac{\epsilon_d'(n+m)(n+m-1)(n-m+1)(n-m+2)}{4n(n+1)} \delta_{nv} \delta_{m-2,u} + \frac{[n(n+1)-m^2]\epsilon_c'}{2n(n+1)} \delta_{nv} \delta_{mu} + \epsilon_3' \delta_{nv} \delta_{mu} + \frac{\epsilon_d'}{4n(n+1)} \delta_{nv} \delta_{m+2,u}. \tag{B1}$$

$$\begin{aligned} \tilde{e}_{uv}^{mn} = {} & \frac{i\epsilon_d'(n-m+1)(n+m)(n+m-1)(n+m-2)}{4n(2n+1)} \delta_{n-1,v} \delta_{m-2,u} + \frac{i\epsilon_c' m(n+m)}{2n(2n+1)} \delta_{n-1,v} \delta_{mu} - \frac{i\epsilon_d'}{4n(2n+1)} \delta_{n-1,v} \delta_{m+2,u} \\ & - \frac{i\epsilon_d'(n-m+1)(n-m+2)(n-m+3)(n+m)}{4(n+1)(2n+1)} \delta_{n+1,v} \delta_{m-2,u} + \frac{i\epsilon_c' m(n-m+1)}{2(n+1)(2n+1)} \delta_{n+1,v} \delta_{mu} + \frac{i\epsilon_d'}{4(n+1)(2n+1)} \delta_{n+1,v} \delta_{m+2,u}. \end{aligned} \tag{B2}$$

$$\begin{aligned} \tilde{f}_{uv}^{mn} = {} & -\frac{i\epsilon_d'(n-m+1)(n+m)(n+m-1)(n+m-2)}{4(2n+1)} \delta_{n-1,v} \delta_{m-2,u} - \frac{i\epsilon_c' m(n+m)}{2(2n+1)} \delta_{n-1,v} \delta_{mu} + \frac{i\epsilon_d'}{4(2n+1)} \delta_{n-1,v} \delta_{m+2,u} \\ & - \frac{i\epsilon_d'(n-m+1)(n-m+2)(n-m+3)(n+m)}{4(2n+1)} \delta_{n+1,v} \delta_{m-2,u} + \frac{i\epsilon_c' m(n-m+1)}{2(2n+1)} \delta_{n+1,v} \delta_{mu} + \frac{i\epsilon_d'}{4(2n+1)} \delta_{n+1,v} \delta_{m+2,u}. \end{aligned} \tag{B3}$$

$$\begin{aligned} \bar{g}_{uv}^{mn} = {} & -\frac{i\epsilon_d'(n+1)(n-m+1)(n+m)(n+m-1)(n+m-2)}{4(n-1)n(2n+1)} \delta_{n-1,v} \delta_{m-2,u} - \frac{i\epsilon_c' m(n+1)(n+m)}{2n(n-1)(2n+1)} \delta_{n-1,v} \delta_{mu} \\ & + \frac{i\epsilon_d'(n+1)}{4n(n-1)(2n+1)} \delta_{n-1,v} \delta_{m+2,u} + \frac{i\epsilon_d' n(n-m+1)(n-m+2)(n-m+3)(n+m)}{4(n+1)(n+2)(2n+1)} \delta_{n+1,v} \delta_{m-2,u} \\ & - \frac{i\epsilon_c' mn(n-m+1)}{2(n+1)(n+2)(2n+1)} \delta_{n+1,v} \delta_{mu} - \frac{i\epsilon_d' n}{4(n+1)(n+2)(2n+1)} \delta_{n+1,v} \delta_{m+2,u}. \end{aligned} \tag{B4}$$

$$\begin{aligned} \bar{e}_{uv}^{mn} = {} & \frac{\epsilon_d'(n+1)(n+m)(n+m-1)(n+m-2)(n+m-3)}{4(n-1)(2n-1)(2n+1)} \delta_{n-2,v} \delta_{m-2,u} - \frac{\epsilon_c'(n+1)(n+m)(n+m-1)}{2(n-1)(2n-1)(2n+1)} \delta_{n-2,v} \delta_{mu} \\ & + \frac{\epsilon_d'(n+1)}{4(n-1)(2n-1)(2n+1)} \delta_{n-2,v} \delta_{m+2,u} - \frac{\epsilon_d'(n-m+1)(n-m+2)(n+m-1)(n+m)(2n^2+2n+3)}{4n(n+1)(2n-1)(2n+3)} \delta_{n,v} \delta_{m-2,u} \\ & + \frac{\epsilon_c'[m^2(2n^2+2n+3)+n(n+1)(2n^2+2n-3)]}{2n(n+1)(2n-1)(2n+3)} \delta_{n,v} \delta_{mu} + \epsilon_3' \delta_{nv} \delta_{mu} - \frac{\epsilon_d'(2n^2+2n+3)}{4n(n+1)(2n-1)(2n+3)} \delta_{n,v} \delta_{m+2,u} \\ & + \frac{\epsilon_d' n(n-m+1)(n-m+2)(n-m+3)(n-m+4)}{4(n+2)(2n+1)(2n+3)} \delta_{n+2,v} \delta_{m-2,u} - \frac{\epsilon_c' n(n-m+1)(n-m+2)}{2(n+2)(2n+1)(2n+3)} \delta_{n+2,v} \delta_{m,u} \\ & + \frac{\epsilon_d' n}{4(n+2)(2n+1)(2n+3)} \delta_{n+2,v} \delta_{m+2,u}. \end{aligned} \tag{B5}$$

$$\bar{f}_{uv}^{mn} = -\frac{\epsilon_d'(n+1)(n+m)(n+m-1)(n+m-2)(n+m-3)}{4(2n-1)(2n+1)}\delta_{n-2,v}\delta_{m-2,u} + \frac{\epsilon_c'(n+1)(n+m)(n+m-1)}{2(2n-1)(2n+1)}\delta_{n-2,v}\delta_{mu}$$
$$-\frac{\epsilon_d'(n+1)}{4(2n-1)(2n+1)}\delta_{n-2,v}\delta_{m+2,u} - \frac{3\epsilon_d'(n-m+1)(n-m+2)(n+m-1)(n+m)}{4(2n-1)(2n+3)}\delta_{n,v}\delta_{m-2,u} - \frac{\epsilon_c'(n^2+n-3m^2)}{2(2n-1)(2n+3)}\delta_{n,v}\delta_{mu}$$
$$-\frac{3\epsilon_d'}{4(2n-1)(2n+3)}\delta_{n,v}\delta_{m+2,u} - \frac{\epsilon_c' n(n-m+1)(n-m+2)}{2(2n+1)(2n+3)}\delta_{n+2,v}\delta_{m,u}$$
$$+\frac{\epsilon_d' n(n-m+1)(n-m+2)(n-m+3)(n-m+4)}{4(2n+1)(2n+3)}\delta_{n+2,v}\delta_{m-2,u} + \frac{\epsilon_d' n}{4(2n+1)(2n+3)}\delta_{n+2,v}\delta_{m+2,u}. \quad \text{(B6)}$$

For the method to derive these matrix elements, the readers are referred to Ref. [12].

[1] E. Yablonovitch, Phys. Rev. Lett. **58**, 2059 (1987).
[2] E. Yablonovitch, T. J. Gmitter, and R. Bhat, Phys. Rev. Lett. **61**, 2546 (1988).
[3] E. Yablonovitch and T. J. Gmitter, Phys. Rev. Lett. **63**, 1950 (1989).
[4] J. D. Joannopoulos, R. D. Meade, and J. N. Winn, *Photonic Crystals* (Princeton University Press, Princeton, 1995).
[5] *Photonic Band Gap Materials*, edited by C. M. Soukoulis (Kluwer, Dordrecht, 1996).
[6] Z. Zhang and S. Satpathy, Phys. Rev. Lett. **65**, 2650 (1990).
[7] K. M. Ho, C. T. Chan, and C. M. Soukoulis, Phys. Rev. Lett. **65**, 3152 (1990).
[8] K. Busch and S. John, Phys. Rev. Lett. **83**, 967 (1999).
[9] A. Moroz, Phys. Rev. B **66**, 115109 (2002).
[10] H. Chen, W. Y. Zhang, Z. L. Wang, and N. B. Ming, J. Phys.: Condens. Matter **16**, 165 (2004).
[11] F. Guan, Z. F. Lin, and J. Zi, J. Phys.: Condens. Matter **17**, L343 (2005).
[12] Z. Lin and S. T. Chui, Phys. Rev. E **69**, 056614 (2004).
[13] Z. F. Li, L. L. Lin, B. Y. Gu, and G. Z. Yang, Physica B **279**, 159 (2000).
[14] Z. Y. Li, B. Y. Gu, and G. Z. Yang, Eur. J. Biochem. **11**, 65 (1999).
[15] X. H. Wang, B. Y. Gu, Z. Y. Li, and G. Z. Yang, Phys. Rev. B **60**, 11417 (1999).
[16] I. H. H. Zabel and D. Stroud, Phys. Rev. B **48**, 5004 (1993).
[17] Z. Y. Li, J. Wang, and B. Y. Gu, Phys. Rev. B **58**, 3721 (1998).
[18] H. S. Sözüer, J. W. Haus, and R. Inguva, Phys. Rev. B **45**, 13962 (1992).
[19] Y. S. Chan, C. T. Chan, and Z. Y. Liu, Phys. Rev. Lett. **80**, 956 (1998).
[20] S. Fan, P. R. Villeneuve, and J. D. Joannopoulos, Phys. Rev. B **54**, 11245 (1996).
[21] A. J. Ward and J. B. Pendry, Phys. Rev. B **58**, 7252 (1998).
[22] J. Korriga, Physica (Amsterdam) **13**, 392 (1947).
[23] W. Kohn and N. Rostoker, Phys. Rev. **94**, 1111 (1954).
[24] K. Ohtaka, Phys. Rev. B **19**, 5057 (1979).
[25] K. Ohtaka, J. Phys. C **13**, 667 (1980).
[26] N. Stefanou and A. Modinos, J. Phys.: Condens. Matter **3**, 8135 (1991).
[27] Y. L. Xu, Appl. Opt. **34**, 4573 (1995).
[28] Y. L. Xu, Appl. Opt. **36**, 9496 (1997).
[29] Y. L. Xu, Phys. Rev. E **67**, 046620 (2003).
[30] A. D. Kiselev, V. Yu. Reshetnyak, and T. J. Sluckin, Phys. Rev. E **65**, 056609 (2002).
[31] J. A. Stratton, *Electromagnetic Theory* (McGraw-Hill, New York, 1941).
[32] C. F. Bohren and D. R. Huffman, *Absorption and Scattering of Light by Small Particles* (John Wiley & Sons, New York, 1983).